An Image Based Overexposed Taillight Detection Method for Frontal Vehicle Detection in Night Vision

Chun-Liang Chien, Hsueh-Ming Hang*, Din-Chang Tseng, and Yong-Sheng Chen
*National Chiao Tung University, Taiwan, R.O.C.
E-mail: hmhang@mail.nctu.edu.tw Tel: +888-3-5714864

***Abstract*—To achieve the goal of frontal vehicle detection in night-driving condition, we propose an effective method to detect the red taillights of vehicles. The challenge is that the taillight images captured with automatic exposure typically are overexposed, which makes red color segmentation often erroneous. Instead of customizing the camera hardware to tackle this problem, we combine morphological and logical operations to extract the overexposed region in taillights, which leads to a much more reliable taillight detection scheme. Then, we develop a robust pairing process that clusters two taillight candidates into a pair that represents a vehicle. Several criteria are considered in the pairing process, including the similarities of area, shape, and height of a pair of lights. In addition, we include the temporal consistency criterion; that is, a pair of taillights should be continually detected for a certain duration of time. An energy function is used to aggregate these criteria together. Our experiments show that both the missing and false detection rates are lower than 1.5%.**

I. INTRODUCTION

When people driving at night, the frontal vehicles are mostly visible by their red-color taillights. Indeed, the worldwide motor regulations [1] specify the color and brightness of taillights. Although the light conditions vary drastically at night, the red taillights are rather robust and stable signals. Vehicular taillights appear as the brightest regions in a monochrome image captured at night; therefore, the simple intensity thresholding method was often used to detect taillights [2-5]. However, the ambient lighting conditions are complicated in the urban area and thus the vehicle taillights are easily confused with the other nonvehicle light sources.

Most nonvehicle light sources can be removed using the color information. The most common approach makes use of the RGB color space [6-10]. Separate RGB thresholds for brightness and redness are implemented in [9]. Whereas in [7], only the red channel of the RGB data is processed. However, in the images captured with automatic exposure, the taillights often appear overexposed.

The task of detecting taillights can be considerably improved by utilizing the new and nonstandard camera hardware [11-13]. O'Malley et al. [14] proposed a two-stage camera configuration. However, a piece of custom hardware may not be used for the other driver-assistance purposes. For example, the static exposure level is unsuitable for the ordinary image capture for dashboard driving recording. Furthermore, the custom hardware also adds cost and complexity to the automobile manufacturing. Finally, only some special cameras have the interface that is configurable by the user.

Instead of customizing the hardware or configuring the exposure control of the camera, we combine morphological and logical operations to extract the overexposed central region of taillight, so that the taillights can be properly segmented. The proposed detection and warning process consists of two procedures. The function blocks of the *taillights detection process* are shaded in green in Fig. 1, and those of the *taillights pairing and range estimation process* are in purple in Fig. 1.

II. OVEREXPOSED REGIONS EXTRACTION (ORE) FILTER

It has been observed that taillight usually appear as white regions with red surroundings as they can partially saturate the image sensors [6, 7]. This "blooming" effect is shown in Fig. 2(a). The perimeter of the overexposed white regions has been discussed in [6]. If the surrounding area is comprised mostly of red pixels, it is considered as a potential taillight. Based on this assumption, both red and white color thresholding are used to segment the taillights. A red and white color thresholding technique has been discussed in [15], where the test image frame is transformed from RGB to HSV color space. After hue, saturation, and value thresholding, the red and white pixels are extracted and marked as the red and gray pixels shown in Fig. 2(b). To extract the overexposed central region, O'Malley et al. [15] uses a binary mask created from the bounding box of the red regions. This mask is applied to the white thresholded image to extract only the white regions that are adjacent to red regions. However, if some non-taillight white pixels appear in the bounding box, they are misclassified as the overexposed central region.

Here, we design an *overexposed regions extraction* (ORE) filter to effectively extract the overexposed central region. First, instead of creating a bounding box of red regions, a morphological CLOSING operation is used to close the central region of the red halo. To properly extract the overexposed region of taillights of a front vehicle, a rectangle is overlaid on the captured area and its size is equal to half of the taillight diameter. As shown in Fig. 2(c), the central overexposed regions are well extracted even though the taillights are falsely connected.

Next, to remove the false-connected areas, a logical AND operator is applied to produce the intersection of the closing region and the high intensity thresholding region. After this operation, the red surrounding and low intensity areas are removed. As the yellow-color pixels shown in Fig. 2(d), the overexposed central regions are effectively extracted and the false connected areas are removed.

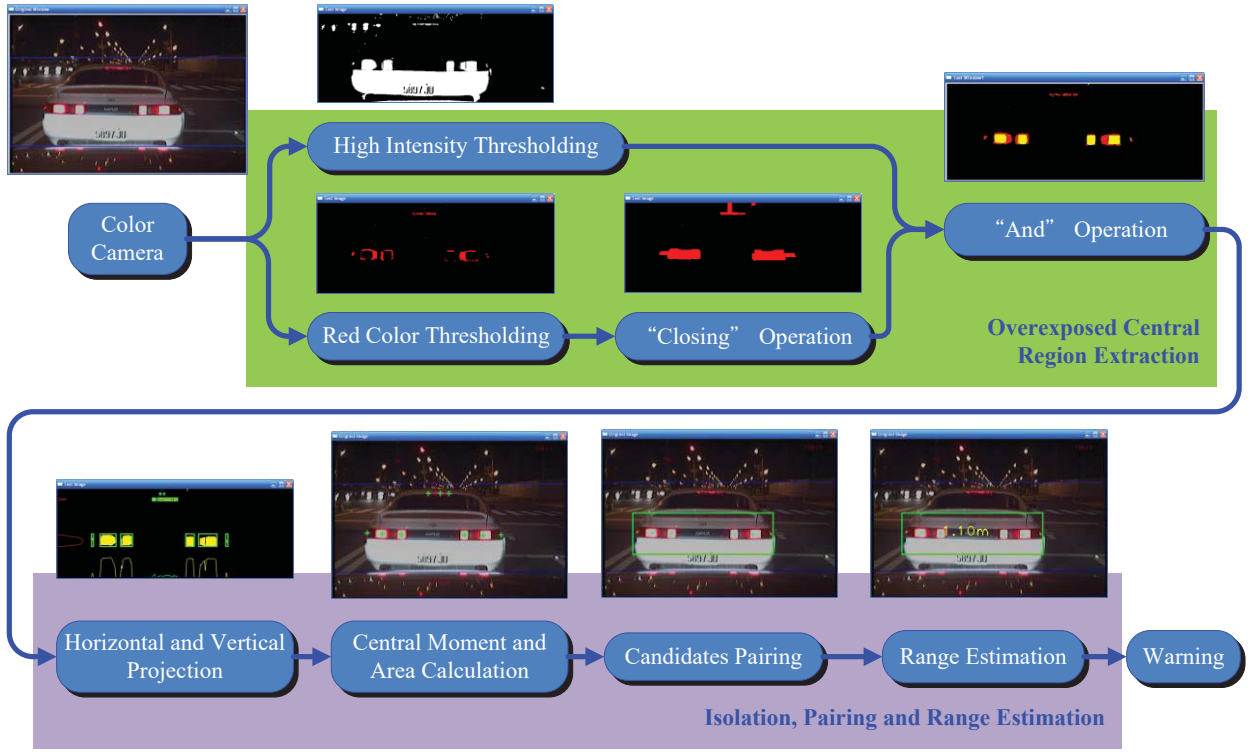

Fig. 1 Flowchart of the proposed frontal vehicle detection and warning system.

Thus, the complete ORE filtering can be described in Algorithm 1.

Algorithm 1 *Overexposed Region Extraction* (*ORE*) *Filter*

Step 1. Identify areas with high intensity (I_{white}) and red color (I_{red}) by thresholding using the predetermined thresholds.

Step 2: Morphological *closing* is applied to I_{red} to obtain a closed image I_{close}

$$\begin{cases} I_{\text{dilate}} = \max\limits_{(x',y')\in kernel} I_{\text{red}}(x+x', y+y') \\ I_{\text{close}} = \min\limits_{(x',y')\in kernel} I_{\text{dilate}}(x+x', y+y') \end{cases} \quad (1)$$

Step 3: The intersection of I_{white} and I_{colse} is extracted by a logical AND operation, which removes the false closed regions and produces the taillight image I_{light}.

$$I_{\text{light}} = \text{Closing}(I_{\text{red}}) \wedge I_{\text{white}} \quad (2)$$

We will need a rather precise estimate of the size of taillights to facilitate the taillights pairing process later. Therefore, the overexposed central region needs to be correctly extracted. In [16, 17], the Nakagami image was used to reduce the scattering noise generated by the non-taillights as shown in Fig. 3. However, the angle between the camera and the taillight must be small. Furthermore, the high reflectance rear bumper cannot be totally removed in the Nakagami image. On the other hand, our proposed method can handle the scattering property of taillights especially when the brake lights are lighted as shown in Fig. 3. If we use the ORE-filter-extracted yellow pixels in Fig. 3(b) to estimate the center, shape, and area of taillights, the light scattering problem can be effectively resolved. Furthermore, this procedure can exclude the nearby high reflectance areas. For example, the white rear bumper shown in Fig. 2(a) are rejected although it is very close to the taillights.

III. Rear Lights Isolation

A pair of rear lights should be horizontally aligned on a captured image. Hence, a horizontal projection of pixels of rear light is used to separate rear lights at different heights as the red curves on the left side of Fig. 4(b). Then, a threshold is applied to create a few horizontal ROIs, which are marked by the yellow horizontal lines in Fig. 4(b). These horizontal ROIs contains pairs of rear lights at different heights. Then, the vertical projection of rear light pixels in each horizontal ROI is generated and one example is shown in Fig. 4(b) as the green curves at the bottom. Likewise, a threshold is used to create bounding boxes marked by the white vertical lines shown in Fig. 4(b). Each box contains an isolated rear light. The sum of the vertical projection in a bounding box is represented as the area of a rear light and the central moment of pixels in a bounding box is calculated below, which is denoted as the central point of a rear light.

$$\begin{cases} \bar{x} = \dfrac{\sum_{x,y} I_{x,y} \cdot x}{\sum_{x,y} I_{x,y}} \\ \bar{y} = \dfrac{\sum_{x,y} I_{x,y} \cdot y}{\sum_{x,y} I_{x,y}} \end{cases} \quad (3)$$

where x and y are the horizontal and vertical pixel coordinates inside a bounding box, respectively. The I_{xy} vlue is set to 1 if

the pixel at (x, y) is a rear light pixel; otherwise, it is 0. Then, $\bar{x}$ and $\bar{y}$ are the coordinates of central moment indicated by the green cross in Fig. 4(a).

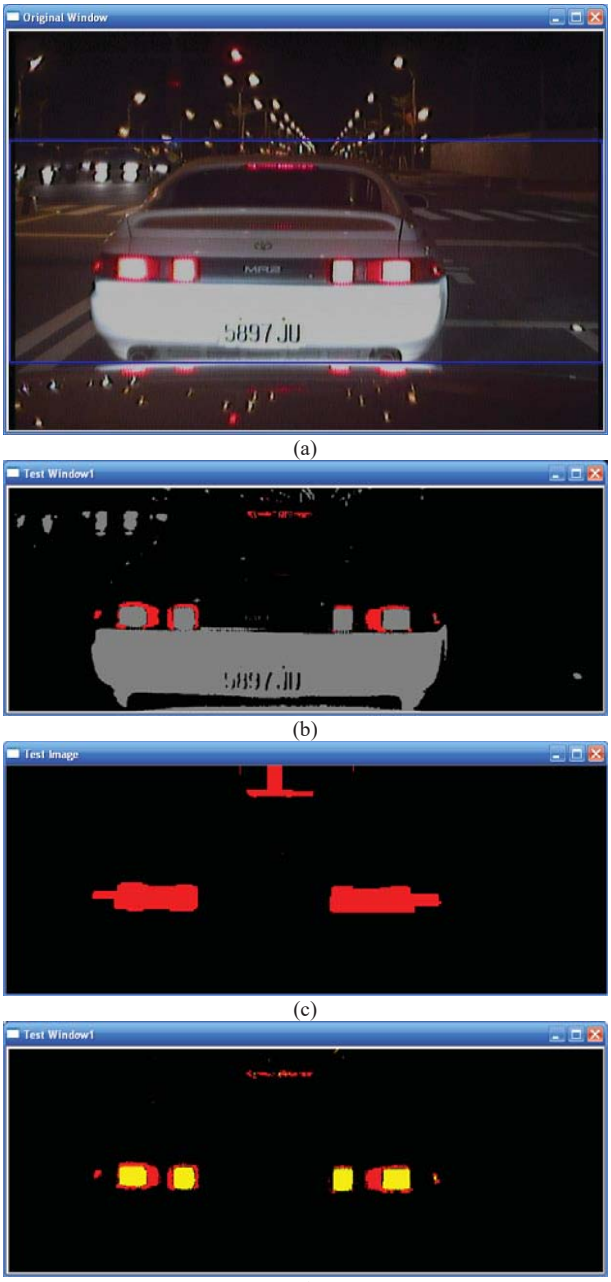

(a)

(b)

(c)

(d)

Fig. 2. The rear light extraction procedure. (a) The original image where the ROI is in the blue box. (b) The red color thresholding result I_{red} and the high intensity thresholding result I_{white}. (c) After the *closing* operation applied to I_{red}. (d) The extract rear lights.

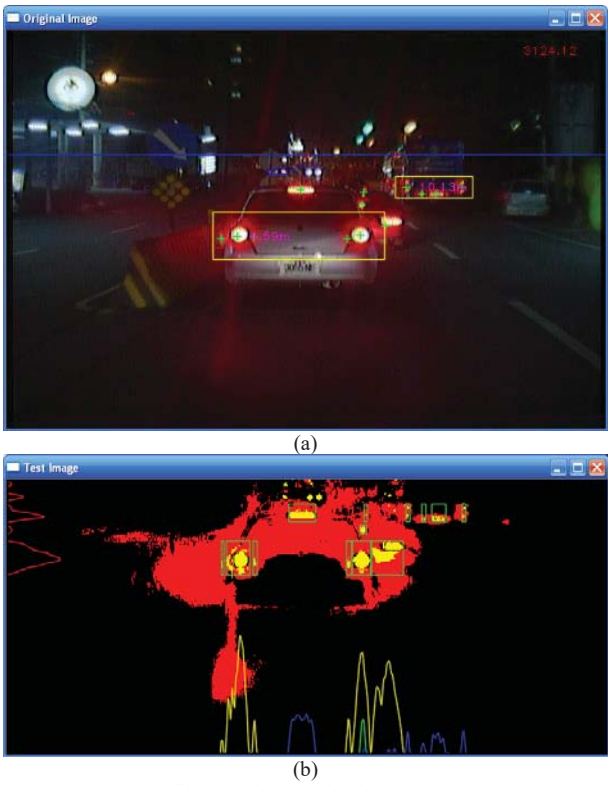

(a)

(b)

Fig. 3. Another ORE filter results. (a) The detection result of near and far front vehicles. (b) The taillights filtering and extraction results of (a).

(a)

(b)

Fig. 4. The rear light segmentation. (a) The original image. (b) After horizontal and vertical projections, the extracted rear lights are enclosed by bounding boxes.

IV. TAILLIGHTS PAIRING

A pair of taillights of a vehicle is usually symmetrical. Hence, a pairing process is designed to identify all pairs of taillights in the captured image. First, three criterions is used to eliminate the impossible pairs. Then, the normalized cross correlation coefficient is used to estimate the likelihood of this pairing.

The first criterion is as follows. If the area difference between two candidates is greater than a threshold, they are not paired. However, the area difference of a near vehicle is greater than that of a faraway one. Hence, a normalized area difference dA_{mn} between candidates m and n is defined below.

$$dA_{mn} = \frac{|a_m - a_n|}{a_m + a_n} \leq 0.2 \tag{4}$$

where a_m and a_n are the areas of candidates m and n, respectively. The value of dA_{mn} is in the range of [0, 1] and the smaller the better. The threshold is set to 0.2 in this work.

Second, if the height difference between two candidates is greater than a threshold, they are not paired. Similarly, the height difference between two candidates should be normalized and we use the *horizontal interval* between a pair of lights to normalize the height difference. The normalized height difference term is defined as follows.

$$dH_{mn} = \frac{|h_m - h_n|}{|x_m - x_n|} \leq 0.1 \tag{5}$$

where h_m and h_n are the vertical coordinates of the centers of candidates m and n, respectively. And x_m and x_n are the horizontal coordinates of the centers of candidate m and n, respectively. We specify that the height difference between a pair of taillights should not exceed 10% of the horizontal interval between two taillights based on our observations.

Third, a pair of candidates with abnormal aspect ratio should also be eliminated. In this work, we assume that the area of a pair of taillight should be proportional to the interval between them. Hence, we propose a ratio R_{mn} of the square of taillight horizontal interval (distance between a pair of taillights) to the average taillight areas as defined below.

$$T_1 \leq \left(R_{mn} = \frac{w^2}{(a_m + a_n)/2} \right) \leq T_2 \tag{6}$$

where a_m and a_n are the area of candidates m and n, respectively, and w is the interval between candidates m and n. From our experiments, the thresholds T_1 and T_2 of most vehicles are 36 and 180, respectively.

If a pair of light candidates pass the aforementioned three criteria, an energy function is calculated to estimate the pairing likelihood probability. In addition to aforementioned area difference dA_{mn} and height difference dH_{mn}, the shape similarity and position tracking are also considered because the shape of a pair of taillights are generally the same. Furthermore, the frontal vehicle taillights should stay at similar positions for a number of frames.

The shape similarity can be evaluated by using the normalized cross correlation coefficient *NCC* [18] as defined below

$$NCC(A,B) = \frac{1}{XY} \sum_{x=0}^{X-1} \sum_{y=0}^{Y-1} A(x_0 + x, y_0 + y) B(x_0 + X - x, y_0 + y) \tag{7}$$

where A and B are two sets of pixels (candidates) to be paired, x_0 and y_0 are the top-left coordinates of the bounding box enclosing A. X is the column pixel numbers between A and B. Y is the row numbers of bounding box enclosing A and B. Note that the "convolution" operation is applied in the x direction due to the typical horizontal symmetrical property of a pair of taillights. The normalized cross correlation coefficient is in the range of [0, 1] and the larger the better. However, the total energy is the smaller the better; hence, the *NCC* item is subtracted from 1 in the energy calculation as shown in Eq. (8).

Finally, the position tracking is included by checking whether there exist previously detected pairs founded in the nearby locations. All successfully paired taillight pairs are stored in a pairing list and each of them is assigned a detected number N_d. If a previously detected pair is founded on the pairing list, its detected number N_d will be attached to this candidate pair and will be used in the energy evaluation. Otherwise, its N_d is equal to 0. After the pairing process is completed, the N_d of the pairs that are not detected in the current frame is decreased by 1; otherwise, it is increased by 1. If the detected number N_d of a successfully paired taillights is equal to 30, it is labeled by a yellow bounding box as shown in Fig. 3(a). To normalize N_d in the range of [0, 1], it is divided by 30 since the maximum of N_d is 30. Next, to match the other energy terms, the normalized N_d is subtracted from 1 in the energy evaluation. The entire pairing energy E_{mn} of a taillight candidate pair (m and n) is defined by Eq. (7). A smaller energy E_{mn} means a higher probability of being a taillight pair.

$$E_{mn} = \frac{|a_m - a_n|}{a_m + a_n} + \frac{|h_m - h_n|}{|x_m - x_n|} + (1 - NCC) + \left(1 - \frac{N_d}{30}\right) \tag{8}$$

V. RANGE ESTIMATION

A forward collision warning (FCW) system in [19] was developed by combining a vehicle detection and a range (distance) estimation algorithms. The range R between the camera and the detected vehicles can be estimated as follows [5].

$$R = \frac{H_{\text{camera}} - H_{\text{light}}}{\tan(\theta + \alpha)} \tag{9}$$

where H_{camera} and H_{light} are the heights of camera and rear light, respectively. θ is the tilt angle of camera, and α is the angle between the rear lights and optic axis as shown in Fig. 5(a). However, the height of rear light varies significantly due to different types of vehicles. Hence, an average height of rear lights used in [5] is only an approximation.

In this work, we use the vehicle width in the captured image to estimate the range of a frontal vehicle. To estimate the range of a detected vehicle based on its width, as shown in Fig. 5(b), the forward range R can be estimated by

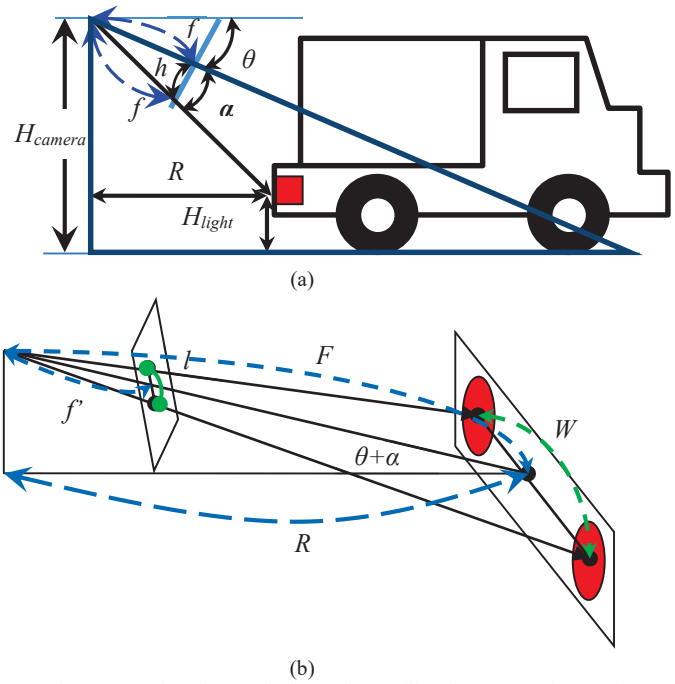

Fig. 5. The range estimation method. (a) The profile of camera and on road vehicle. (b) The schematic diagram of distance calculation.

$$R = F\cos(\theta + \alpha) \tag{10}$$

where θ and α are defined in Fig.5, and F is the distance between the center of vehicle and the center of camera lens. As shown in Fig. 5(a), α can be derived as

$$\alpha = tan^{-1}\left(\frac{h}{f}\right) \tag{11}$$

where h is the distance between the center of rear light and the horizontal central line in image and f is the focal length of camera. Then, F can be derived from their geometrical relationship.

$$\frac{F}{f'} = \frac{W}{l}, \quad F = \frac{f'W}{l} \tag{12}$$

where W is a presumed vehicle width and l is the interval between a pair of rear lights on image. On the other hand, f' can be obtained by

$$f' = \frac{f}{\cos\alpha} \tag{13}$$

Substituting Eqs. (11), (12), and (13) into Eq. (10) yields

$$\begin{aligned} R &= \frac{fW}{l\cos\alpha}(\cos\theta\cos\alpha - \sin\theta\sin\alpha) \\ &= \frac{W}{l}(f\cos\theta - h\sin\theta) \end{aligned} \tag{14}$$

However, the vehicle width W varies from 1.5m to 2.5m for different type of vehicles. In this work, the vehicle width is assumed to be 1.7m (medium value) and the range error caused by this presumed vehicle width will be discussed in next Section.

VI. Range Error Due to Presumed Vehicle Width

The vehicle width is typically in the range of 1.5m (a mini sedan) to 2.5m (a truck). The width of most popular sedans is about 1.7m. Since the width of a vehicle can vary from 1.5m to 2.5m, an estimated range based on a fixed width was reported having only about 70% accuracy [20]. To study more precisely the range error due to vehicle width variation, let the actual vehicle width W' be equal to $W+\delta$, where δ is the difference between the actual vehicle width and the presumed vehicle width. From Eq. (14), the vehicle width l' in an image is

$$\begin{aligned} l' &= \frac{(W+\delta)}{R}(f\cos\theta - h\sin\theta) \\ &= l + \frac{\delta}{R}(f\cos\theta - h\sin\theta) \end{aligned} \tag{15}$$

Hence, the estimated range R' can be derived by substituting Eq. (15) into Eq. (14) to yield

$$R' = \frac{W(f\cos\theta - h\sin\theta)}{l + \delta(f\cos\theta - h\sin\theta)/R} = \frac{R}{1 + \delta/W} \tag{16}$$

For example, the presumed vehicle width is 1.7m, if a frontal mini sedan (1.5m) is detected, the estimated range is equal to $R/(1 - 0.2/1.7) \approx R/0.88$. On the other hand, if a frontal truck (2.5m) is detected, then the estimated range is equal to $R/(1 + 0.8/1.7) \approx R/1.47$. The relationship between R' and δ is shown in Fig. 6. We observed that if δ is larger than 0 (i.e., the actual vehicle width is larger than the presumed vehicle width), then the range error is smaller (e.g., as shown in Fig. 6, ΔR_2 is smaller than ΔR_1). Furthermore, the range is underestimated; that is, the estimated range is smaller than the actual range. Hence, the driver receives an early warning, which is overly cautious but safer.

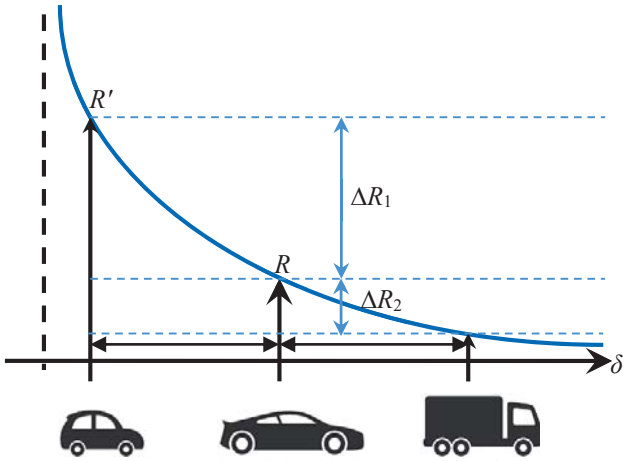

Fig. 6. The relationship between R' and δ.

On the other hand, if the presumed vehicle width is larger than the actual vehicle width, the range error is larger and the range is overestimated; that is, the actual range is smaller than the estimated range. This may lead to a dangerous situation, because the driver receives a late warned message. Hence, a smaller presumed vehicle width is better.

Based on the safety consideration, a conservative choice is setting the presumed vehicle width to 1.5m. However, the

frontal range of a truck (2.5m) will then be seriously underestimated. Therefore, a more appropriate choice is setting the presumed vehicle to 1.7m because most on-road vehicles are sedans (i.e., W = 1.7m). In practical implementation, the default presumed vehicle width is set to 1.7m and it can be automatically switched to 1.5m based on the speed of vehicle.

VII. System Calibration

In practical situation, it is not easy to obtain f and θ. Hence we use a calibration process to obtain these two fixed values. If we assume the vehicle width W is also a fixed value, Eq. (14) can be represented by

$$R = \frac{C_1 - hC_2}{l} \tag{17}$$

where $C_1 = Wf\cos\theta$ and $C_2 = W\sin\theta$. In a practical calibration process, a pair of red LEDs are used to simulate a pair of vehicle rear lights and the interval between these two LEDs is equal to our presumed vehicle width, i.e., 1.7m. We placed LEDs at n different ranges; thus, Eq. (17) is repeated n times and can be concatenated into a vector-matrix form.

$$\begin{bmatrix} R_1 l_1 \\ \vdots \\ R_n l_n \end{bmatrix} = \begin{bmatrix} 1 - h_1 \\ \vdots \\ 1 - h_n \end{bmatrix} \begin{bmatrix} C_1 \\ C_2 \end{bmatrix} \Rightarrow \mathbf{R} = \mathbf{HC} \tag{18}$$

Then, C_1 and C_2 can be derived by using the least squared error method as follows

$$\mathbf{C} = (\mathbf{H}^T\mathbf{H})^{-1}\mathbf{H}^T\mathbf{R} \tag{19}$$

After C_1 and C_2 are obtained, the range value based on a pair of detected rear lights can be estimated by Eq. (17).

VIII. Experimental Results

In this work, a Hitachi KP-F3 camera is in use, which has a physical pixel size of 7.4 μm(H) × 7.4 μm(V) and the image resolution is 640 × 480. Its focal length f is 15 mm and the tilt angle θ is equal to 10°. All captured videos are processed on a desktop computer and it is equipped with Intel Core2 Duo CPU E8400 3.0GHz and 3.46GB RAM. We use the Microsoft Visual C++ 2008 for coding and the OpenCV 2.1 library for decoding video, processing images and displaying the final results. We set a region-of-interest (ROI), whose height is half of the image height and is above the car hood. The whole algorithm can be completed in 1/30 second. Not only the near frontal vehicles but also the farther ones can be correctly detected as shown in Fig. 7(a). The detection rate is high even under dark night-driving condition. On the other hand, in the urban streets, the complex environment lights can be effectively filtered out and the taillights are correctly extracted and detected, and they are successfully paired as shown in Fig. 7(b).

A. Tracking-Based Detection

Rear lights are easily mistakenly paired when two vehicles run in parallel and their rear lights are similar as shown in Fig. 8(a). Furthermore, when the turn signal is on, the area of rear light is expanded as shown in Fig. 8(b). Under these conditions, the shape, area and height information of rear light are not sufficient to pair all candidates correctly. To increase accuracy, as discussed in Sections IV, the detected number of a rear light pair in the previous 30 frames is considered as a weighting factor in the pairing process. Hence, the pairing result is less interfered by a new coming vehicle as in the case shown in Fig. 8(a). On the other hand, a successfully paired rear light pair is eliminated when it is not detected for 30 frames. The duration of turn signal is often shorter than 30 frames, and thus a pair of detected rear lights can be correctly tracked as shown in Fig. 8(b).

(a)

(b)

Fig. 7. The experimental results. (a) The detection result under low street light condition. (b) The detection result in a complex ambient light environment.

B. False Alarm and Missed Detection

To evaluate the type I error (false alarm) and type II error (miss), videos under different lighting conditions were collected including both the urban and the highway environments. For the FCW application, the missing rate is the ratio of the number of "missing" frames to the total number of frames. The false alarm rate is the ratio of the number of "falsely detected" frames (no front vehicles in the forward collision warning range) to the total number of frames.

(a)

(b)

Fig. 8. The experimental results of (a) two vehicles run in parallel. (b) The size of a rear light pair is different when the turn signal is on.

The range estimation error is difficult to evaluate under the dynamical true road condition unless we compare the estimation result with the data provided by a laser range finder. Although we do not have a laser range finder, the estimated range values in our experiments seem to match the human inspection. The key performance of our system is the high correct detection rate. Our experimental results are listed in Table I. Both types of error rates are less than 2% for total 13 min (23280 frames) test video.

TABLE I.
SUMMARY OF EXPERIMENTAL RESULTS

False Alarm (False Positive) Rate (%)	299 / 23280 = 1.284%
Missed Detection (False Negative) Rate (%)	310 / 23280 = 1.33%

IX. DISCUSSIONS

As described in Section IV, the thresholds of qualifying terms can be selected based on the safety requirement. If the threshold is small, the missing probability increases but the false alarm probability decreases. It would be the opposite if the threshold is large. To reduce the missing probability, we set the threshold as high as possible until the false alarms is intolerable. Here, we discuss some missed detection and false alarm cases.

A. *Missed Detection Cases*

We examine the missed detection cases and find that one main cause is that the rear light is not very red as shown in Fig. 9(a). Then, the overexposed central region of the rear light cannot be well extracted. That is, if most of the rear light pixels are not classed to red pixels as shown by the yellow circle in Fig. 9(b), the overexposed central region cannot be correctly identified after the closing operation. Furthermore, if the rear light is not red, for example, the light cover is broken or faded, the overexposed extraction algorithm may thus fail. There are other missed detection cases. For example, one of the rear light pair of a frontal vehicle is outside the image because the frontal vehicle is turning to left or right as shown in Fig. 9(c).

B. *False Alarm Cases*

Most false alarms occur in the urban streets due to the complex lighting conditions. However, under the traffic jammed condition, the complex rear light distribution can lead to mispairing as shown by the left-side green bounding box in Fig. 10(a). As we can see that the left rear light of a car is obstructed by a scooter rider and thus the unobstructed right light is paired with the right light of another front vehicle inside the green circle in Fig. 10(b). Fortunately, this front vehicle is on the left lane. The middle front vehicle is correctly detected and this false alarm can thus be neglected.

C. *Double Lights Cases*

Another abnormal detection is caused by double rear lights. As shown in Fig. 11(a), a duplicate pairing result is produced due to the vertically double rear lights. However, the range of the frontal vehicle can still be correctly estimated. Hence, this case is not a serious problem and it may be resolved by checking whether the bounding boxes of two pairs of rear lights are overlapped in the vertical directions. Fig. 11(b) shows a case of horizontal double lights. The pairing process is easily confused by the horizontal double rear lights due to their similar shape and close position. If one of the inner rear light is paired, the range of the frontal vehicle may be overestimated. Also, the inner and outer lights may interfere each other in the pairing process. In the future work, we may be able to reduce this type of errors by imposing additional checks based on the observations here.

X. CONCLUSIONS

In this paper, a frontal vehicle detection method is proposed particularly for night vision. The main cue we use in the evening frontal vehicle detection is identifying a pair of taillights. Several steps are needed to produce a reliable taillight pair detection. We first propose a simple yet effective extraction algorithm that extracts the overexposed central region of taillights. Then, the extracted regions are clustered and identified to be a pair of taillights belonging to a frontal vehicle. A deliberate pairing process is developed to pair the detected taillight candidates. In our experiments, the proposed method can effectively detect almost all vehicles under no-rain night-driving condition. Both the missing and the false alarm probabilities are under 1.5%. In addition, there are other

interesting problems to be further explored. For example, how to estimate the range of one taillight vehicle such as the scooter is still an open problem.

(a)

(b)

(c)

Fig. 9. The wrong pairing results under traffic jamming condition. (a) The detection result in traffic jammed condition. (b) The rear lights filtering and extraction results of (a). (c) One of the rear light pair is outside the image because the frontal vehicle is turning to left.

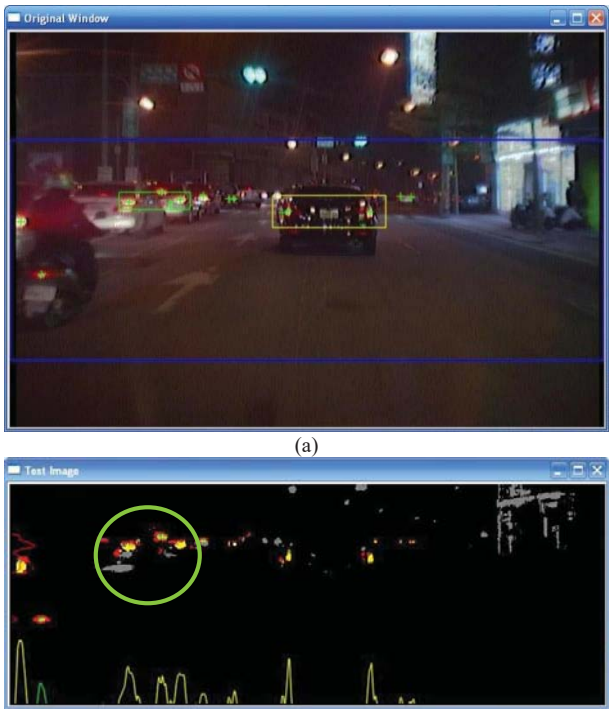

(a)

(b)

Fig. 10. A false alarm case due to obstructed rear lights. (a) The detection result in the multiple obstructed vehicle condition. (b) The rear lights filtering and extraction results of (a).

(a)

(b)

Fig. 11. Some missed detection examples of double lights. (a) The detection result of vehicle with vertical double lights. (b) The detection result of vehicle with horizontal double lights.

REFERENCES

[1] "Federal Motor Vehicle Safety Std. 108," *Nat. Highway Traffic Safety Admin., Tech. Rep.*

[2] S. Kim, S.-Y. Oh, J. Kang, Y. Ryu, K. Kim, S.-C. Park*, et al.*, "Front and rear vehicle detection and tracking in the day and night times using vision and sonar sensor fusion," in *IEEE/RSJ International Conference on Intelligent Robots and Systems (IROS), 2005.* , 2005, pp. 2173-2178.

[3] N. Alt, C. Claus, and W. Stechele, "Hardware/software architecture of an algorithm for vision-based real-time vehicle detection in dark environments," presented at the Proceedings of the conference on Design, automation and test in Europe, Munich, Germany, 2008.

[4] S. Kim, "Fast vision-based vehicle detection algorithm using recognition of light pattern," *Proc. SPIE,* vol. 4115, p. 654, 2000.

[5] P. F. Alcantarilla, L. M. Bergasa, P. Jimenez, M. A. Sotelo, I. Parra, D. Fernandez*, et al.*, "Night time vehicle detection for driving assistance lightbeam controller," in *IEEE Intelligent Vehicles Symposium, 2008* 2008, pp. 291-296.

[6] M.-Y. Chern and P.-C. Hou, "The lane recognition and vehicle detection at night for a camera-assisted car on highway," in *IEEE International Conference on Robotics and Automation, 2003. Proceedings. ICRA '03.* , 2003, pp. 2110-2115 vol.2.

[7] M. Betke, E. Haritaoglu, and L. S. Davis, "Real-time multiple vehicle detection and tracking from a moving vehicle," *Machine Vision and Applications,* vol. 12, pp. 69-83, 2000.

[8] Y.-L. Chen, "Nighttime vehicle light detection on a moving vehicle using image segmentation and analysis techniques," *W. Trans. on Comp.,* vol. 8, pp. 506-515, 2009.

[9] R. Sukthankar, "RACCOON: A Real-time Autonomous Car Chaser Operating Optimally At Night," in *Intelligent Vehicles '93 Symposium*, 1993, pp. 37-42.

[10] C.-C. Wang, S.-S. Huang, and L.-C. Fu, "Driver assistance system for lane detection and vehicle recognition with night vision," in *IEEE/RSJ International Conference on Intelligent Robots and Systems (IROS), 2005.*, 2005, pp. 3530-3535.

[11] A. López, J. Hilgenstock, A. Busse, R. Baldrich, F. Lumbreras, and J. Serrat, "Nighttime Vehicle Detection for Intelligent Headlight Control." vol. 5259, J. Blanc-Talon, S. Bourennane, W. Philips, D. Popescu, and P. Scheunders, Eds., ed: Springer Berlin / Heidelberg, 2008, pp. 113-124.

[12] C. Schadel and D. Falb, "SmartBeam--A high-beam assist," in *Proc. Int. Symp. Automotive Lighting*, Darmstadt, Germany, 2007.

[13] J. H. Bechtel, J. S. Stam, and J. K. Roberts, "Vehicle vision based systems having improved light source distinguishing features," ed: U.S. Patent 7 408 136 B2 2008.

[14] R. O'Malley, E. Jones, and M. Glavin, "Rear-Lamp Vehicle Detection and Tracking in Low-Exposure Color Video for Night Conditions," *IEEE Transactions on Intelligent Transportation Systems,* vol. 11, pp. 453-462, 2010.

[15] R. O'malley, M. Glavin, and E. Jones, "Vehicle Detection at Night Based on Tail-Light Detection," 2008.

[16] D.-Y. Chen, Y.-H. Lin, and Y.-J. Peng, "Nighttime Brake-Light Detection by Nakagami Imaging," *IEEE Transactions on Intelligent Transportation Systems,* vol. 13, pp. 1627-1637, 2012.

[17] D.-Y. Chen, Y.-J. Peng, L.-C. Chen, and J.-W. Hsieh, "Nighttime Turn Signal Detection by Scatter Modeling and Reflectance-Based Direction Recognition," *Sensors Journal, IEEE,* vol. 14, pp. 2317-2326, 2014.

[18] R. C. Gonzalez and R. E. Woods, *Digital image processing*: Prentice Hall, 2007.

[19] E. Dagan, O. Mano, G. P. Stein, and A. Shashua, "Forward collision warning with a single camera," 2004, pp. 37-42.

[20] I. Gat, M. Benady, and A. Shashua, "A monocular vision advance warning system for the automotive aftermarket," ed. New York, NY, ETATS-UNIS: Society of Automotive Engineers, 2005, p. 8.